MEDIAN PLANE MAGNETIC FIELD DUE TO A PAIR OF CIRCULAR ARC CURRENTS

and

A SOURCE TO PULLER PROGRAM FOR THE CALCULATION OF ION TRAJECTORIES

By

Stephen Joseph Motzny

A THESIS

Submitted to
Michigan State University
in partial fulfillment of the requirements
for the degree of

MASTER OF SCIENCE

Department of Physics

1978

ABSTRACT

MEDIAN PLANE MAGNETIC FIELD DUE TO A PAIR OF CIRCULAR ARC CURRENTS

and

A SOURCE TO PULLER PROGRAM FOR THE CALCULATION OF ION TRAJECTORIES

By

Stephen Joseph Motzny

An expression for the median plane magnetic field due to a pair of circular arc currents is derived, as well as an expression for the average field associated with this geometry. The expressions, which involve incomplete and complete elliptic integrals, respectively, are used to find the fields for a sample problem and the results are compared with values obtained by an alternate technique.

A computer program for the calculation of ion trajectories in the source to puller region of a cyclotron has been written. The program, called TRAJECTORY, assumes a homogeneous magnetic field and uses measured electric fields. The equations of motion are numerically integrated in Cartesian coordinates with τ as independent variable via a fourth order Runga-Kutta progress. Interpolation of fields and potentials involves a double-weighted three-point routine. TRAJECTORY's orbit predictions are in excellent agreement with a case which can be solved analytically and also with the predictions of the orbit code CYCLONE. Using TRAJECTORY, the energy gain and transit time across the first acceleration gap is studied for several values of the dimensionless parameter χ.

ACKNOWLEDGMENT

I am indebted to Dr. M. M. Gordon for his invaluable advice and constant support throughout the writing of this thesis. I would also like to thank Dr. H. G. Blosser for initially directing me toward source to puller studies and Dr. J. Bishop for his help in "getting started."

I wish to thank the cyclotron computer staff for keeping the Sigma-Seven in operation (most of the time) and their advice in programming matters.

I would also like to express my appreciation toward Mary Lynn Devito who helped in the typing of the rough draft. My deepest gratitude goes to Sharon Ledebuhr whose patience in typing the final draft will always be appreciated.

A special thanks goes to my roommates for putting up with me at times, to my friends for their support and encouragement, and to the Nuclear Beer group for making Friday afternoons enjoyable.

Finally, I would like to thank my family, whose constant love and support have made everything possible.

TABLE OF CONTENTS

	Page
LIST OF TABLES.	iv
LIST OF FIGURES	v
1. INTRODUCTION	1
2. MEDIAN PLANE MAGNETIC FIELD DUE TO A PAIR OF CIRCULAR ARC CURRENTS	3
2.1 Introduction	3
2.2 Derivation of the Median Plane Magnetic Field	4
2.3 Sample Problem	10
3. A SOURCE TO PULLER PROGRAM FOR THE CALCULATION OF ION TRAJECTORIES	23
3.1 Introduction	23
3.2 Description of the TRAJECTORY Program.	24
3.2.1 Equations	24
3.2.2 Runga-Kutta Integration	29
3.2.3 Fields and Potentials	29
3.2.4 Input-Output Features	31
3.3 Reliability of TRAJECTORY.	32
3.3.1 Comparison with Analytic Solution	33
3.3.2 Comparison with CYCLONE	37
3.4 Source to Puller Calculations in a Measured Electric Field	39
LIST OF REFERENCES	49

LIST OF TABLES

Table		Page
2.1	Fourier decomposition of the median plane magnetic field for the sample problem being considered. Radius is in inches and $\langle B_z \rangle$, B_3, B_6, etc., are given in gauss.	15
2.2	Median plane magnetic field along $\theta = 0^\circ$ for the sample problem being considered. This table compares B_z for the exact case with five different segmented cases (see text). The numbers in parentheses indicate computer run times in minutes. Radius is in inches and fields are in gauss.	21
3.1	Comparison of TRAJECTORY and the analytic solution for the first harmonic acceleration of $^{14}N^{4+}$ through homogeneous magnetic and electric fields	36
3.2	Comparison of TRAJECTORY and CYCLONE for the first harmonic acceleration of $^{14}N^{4+}$ through a homogeneous magnetic field and a measured electric field, 1.06.5-A.	38

LIST OF FIGURES

Figure		Page
2-1	Geometry considered in the derivation of the median plane magnetic field due to a pair of circular arc currents.	5
2-2	Geometry of the sample problem to be considered. Each circular arc shown actually represents a pair of circular arcs at z = ±1.0 inch. The current, I = 100 amps, is in a counter-clockwise sense	11
2-3	Equi-B-field contours for the median plane magnetic field of the sample problem being considered. The contours extend from -6.5 gauss to +8.5 gauss in 0.5 gauss steps.	14
2-4	Geometry to be considered when calculating the field due to a line segment. The wire has length a, and is located at z = +z'. The current, I, flows in the positive ϑ' direction. The field is first calculated in the primed system and then a transformation is made to the unprimed system (see equations (14)-(16))	18
2-5	Relation between the radius of a circle, r, and the location of a straight line segment, r', subtending the same angle such that the arc length equals the segment length	18
3-1	$\varepsilon \equiv E_{kin}/q\Delta V$ at the puller vs. initial R.F. time for χ-values of .05, .10, .15, and .20. For each χ, curves are plotted for h = 1, 2, 3, and 4	42
3-2	$\varepsilon \equiv E_{kin}/q\Delta V$ at the puller vs. initial R.F. time for χ-values of .30, .40, .50, and .60. For each χ, curves are plotted for h = 1, 2, 3, and 4	43

Figure Page

3-3 Some predicted trajectories for ions with χ = .4 through field 1.06.5-A. The ions making it through the puller are running in the h = 1 mode, and those being pushed back to the source are running in the h = 4 mode. Both cases are plotted for R.F. starting times of $\tau_0 = -20^0, -30^0, -40^0$ and -50^0. The trajectories are superimposed on a 2% contour map of the equipotential lines. The scale is 8:1. 44

3-4 Maximum ε at the puller vs. χ for accelerating modes of h = 1, 2, 3, and 4. 47

3-5 Initial R.F. time τ_0 and transit time $\Delta\tau$ vs. χ for the cases that give maximum source to puller energy gain. Results are again shown for h = 1, 2, 3, and 4. 48

1. INTRODUCTION

The Accelerator Physics group at the Michigan State University Cyclotron Laboratory has directed the bulk of its attention in the last few years to the development of the $K^{\dagger}$= 500 MeV Superconducting Cyclotron. My involvement with the group has introduced me to a very interesting area of research from which the topics of this thesis were chosen.

The first part of this thesis, Section 2, is related to the magnetic fields produced by the trimming coils for the K = 500 MeV machine. The geometry of these coils is such that the segments that are parallel to the median plane are in the form of circular arcs. It has been usual practice to obtain the field from such arcs by appoximating them as being composed of several short line segments connected end to end. Section 2 investigates a completely analytic solution to the circular arc problem and then studies the utility of the resulting expression in solving a sample problem.

Most of my work with the Accelerator Physics group was involved with central region calculations and, in particular, with problems

---

†K refers to the specifications of the cyclotron magnet. The non-relativistic energy of a particle of charge q and mass m moving in a magnetic field of strength B at a radius ρ is given by

$$E = \tfrac{1}{2} B^2 \rho^2 (q^2/m) = K(Q^2/A).$$

With B = 48 kG, ρ = 26 inch, then K $\simeq$ 500 MeV.

related to acceleration across the first gap (i.e., the ion-source to puller-electrode region). For the purpose of these studies, a computer program for the calculation of ion trajectories in this region was written. In the second part of this thesis, Section 3, the program is described, tested, and then used for a few simple, but useful, calculations.

2. MEDIAN PLANE MAGNETIC FIELD DUE TO A PAIR OF CIRCULAR ARC CURRENTS

2.1 Introduction

The trim coil windings for the K = 500 MeV Superconducting Cyclotron under construction at Michigan State University will be wrapped around the pole tips in such a way that the segments of the windings that are parallel to the median plane form circular arcs with their centers of curvature coinciding with the machine center. When calculating the median plane magnetic field due to the trim coils, the circular arcs can be taken in pairs. One circular arc of the pair will be from an upper pole tip at z = +z' and the other arc of the pair will be from a lower pole tip at z = -z', and these arcs will be symmetric with respect to the median plane. This geometry simplifies the problem by eliminating all but the z-component of the median plane field. It is the purpose of this section to derive an exact expression for the median plane magnetic field due to such a pair of circular arc currents.

It will be found that this expression involves incomplete elliptic integrals of the first and second kind. There are many computer subroutines available for the rapid evaluation of these integrals. One such routine will be described in Section 2.3 where the derived expression will be used to calculate the median plane magnetic field for a sample problem.

It is also of interest to obtain an expression for the average magnetic field due to a pair of circular arc currents. This expression

will be found to involve complete elliptic integrals of the first and second kind. In the study of the sample problem in Section 2.3, this expression will be checked.

2.2 Derivation of the Median Plane Magnetic Field

Keeping the notation the same as Smith[1], we consider a pair of circular arc currents (see Figure 2-1), one at $z = +z'$ and the other at $z = -z'$. Both arcs have a radius of curvature L with their centers lying on the $\hat{z}$-axis, and both arcs extend from $\theta = \theta'_1$, to $\theta = \theta'_2$. We wish to calculate the median plane magnetic field due to these currents at a distance ρ from the $\hat{z}$-axis and at an angle θ with respect to $\hat{x}$-axis.

We begin by writing down the Biot-Savart Law,

$$\vec{B} = \frac{\mu_0 I}{4\pi} \int_{C'} \frac{\vec{dl} \times (\vec{r} - \vec{r}')}{|\vec{r} - \vec{r}'|^3} ,$$

and then consider contributions to the integral from both arcs making up the pair simultaneously. A "+" subscript will indicate variables associated with the upper arc and a "-" subscript will indicate variables associated with the lower arc. From Figure 2-1, we see that

$$\vec{r} = \rho \cos\theta \, \hat{x} + \rho \sin\theta \, \hat{y} ,$$

$$\vec{r}'_{\pm} = L \cos\theta' \, \hat{x} + L \sin\theta' \, \hat{y} \pm z' \, \hat{z} ,$$

$$\vec{dl}'_{\pm} = -L \sin\theta' \, d\theta' \, \hat{x} + L \cos\theta' \, d\theta' \, \hat{y} .$$

Hence,

$$\vec{r} - \vec{r}'_{\pm} = (\rho \cos\theta - L \cos\theta')\hat{x} + (\rho \sin\theta - L \sin\theta')\hat{y} \mp z' \hat{z} ,$$

and

$$\vec{dl}'_{\pm} \times (\vec{r} - \vec{r}'_{\pm}) = \mp z' L \cos\theta' \, d\theta' \, \hat{x} \mp z' L \sin\theta' \, d\theta' \, \hat{y} - [L \cos\theta' (\rho \cos\theta - L \cos\theta') + L \sin\theta' (\rho \sin\theta - L \sin\theta')] d\theta' \hat{z}.$$

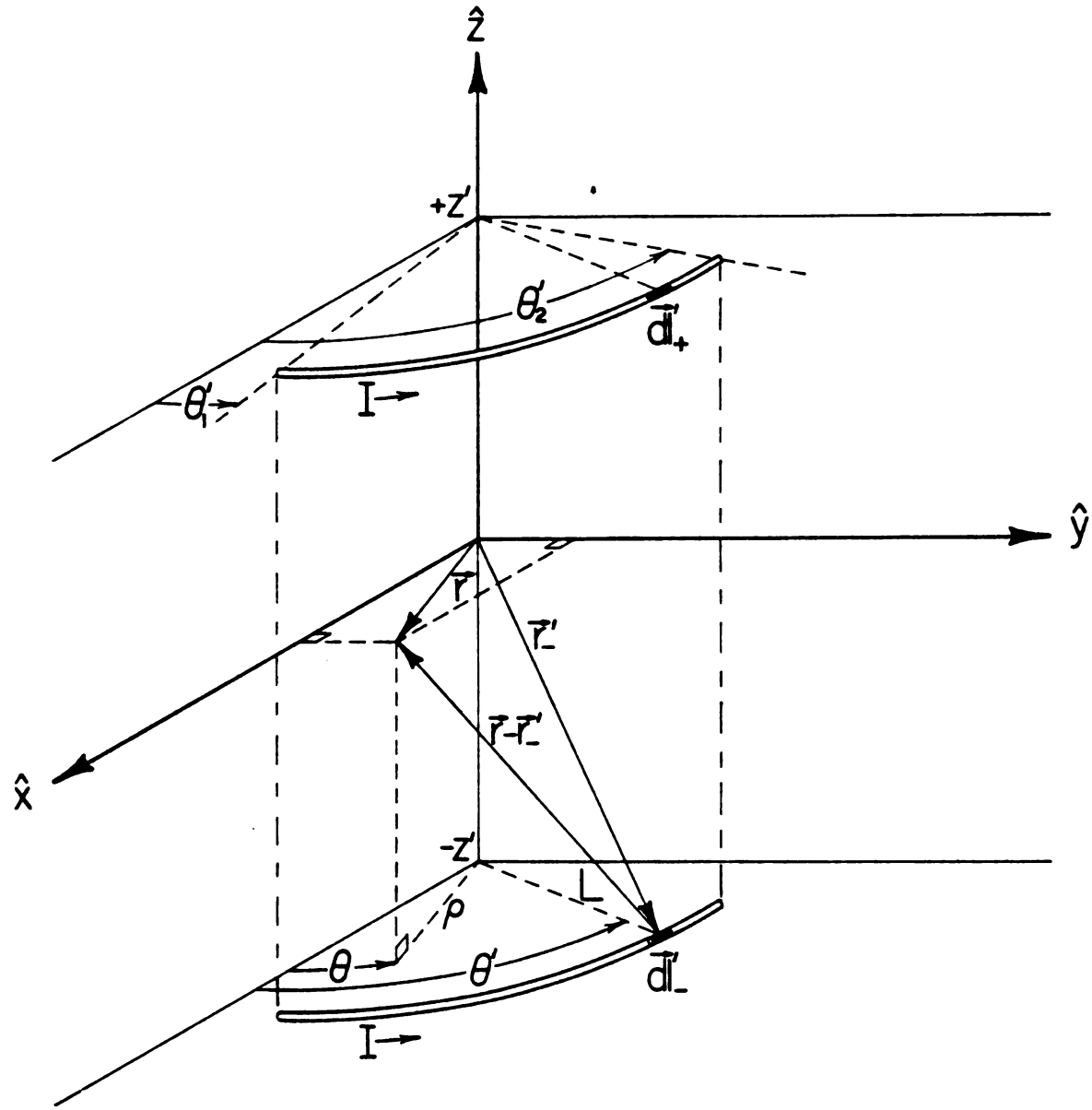

Figure 2-1.--Geometry considered in the derivation of the median plane magnetic field due to a pair of circular arc currents.

Adding the contributions from the upper and lower arcs, we see that only the z-component will survive giving us

$$\begin{aligned}\vec{dl}' \times (\vec{r} - \vec{r}') &= \vec{dl}'_{+} \times (\vec{r} - \vec{r}'_{+}) + \vec{dl}'_{-} \times (\vec{r} - \vec{r}'_{-}) \ , \\ &= -2\,[L\rho\,(\cos\theta'\cos\theta + \sin\theta'\sin\theta) - L^2]\,d\theta'\,\hat{z} \\ &= 2\,[L^2 - L\rho\cos(\theta' - \theta)]\,d\theta'\,\hat{z} \ .\end{aligned}$$

The quantity $|\vec{r} - \vec{r}'_{\pm}|$ can be seen to be

$$|\vec{r} - \vec{r}'_{\pm}| = [L^2 + \rho^2 + z'^2 - 2L\rho\ \cos(\theta' - \theta)]^{\frac{1}{2}} \ .$$

Substitution of the above results into the Biot-Savart Law gives

$$B_z = \frac{\mu_0 I}{2\pi} \int_{\theta'_1}^{\theta'_2} \frac{[L^2 - L\rho\cos(\theta' - \theta)]\,d\theta'}{[L^2 + \rho^2 + z'^2 - 2L\rho\ \cos\,(\theta' - \theta)]^{3/2}} \qquad (2.1)$$

As a start to put this integral in a more recognizable form we let $\theta' - \theta = \pi + 2\phi$, so that, $d\theta' = 2d\phi$, and $\cos(\theta' - \theta) = 2\sin^2\phi - 1$.

Then, $$B_z = \frac{\mu_0 I}{2\pi} \int_{\phi_1}^{\phi_2} \frac{[2L^2 - 2L\rho\,(2\sin^2\phi - 1)]\,d\phi}{[L^2 + \rho^2 + z'^2 - 2L\rho\,(2\sin^2\phi - 1)]^{3/2}} \ ,$$

where $$\phi_1 = \frac{\theta'_1 - \theta}{2} - \frac{\pi}{2} \ ,$$

and $$\phi_2 = \frac{\theta'_2 - \theta}{2} - \frac{\pi}{2} \ .$$

We can write B_z as (temporarily dropping the limits of integration),

$$B_z = \frac{\mu_0 I}{2\pi\,[(L + \rho)^2 + z'^2]^{\frac{1}{2}}} \int \frac{\left[\dfrac{2L^2 + 2L\rho}{(L + \rho)^2 + z'^2} - \dfrac{4L\rho}{(L + \rho)^2 + z'^2}\sin^2\phi\right] d\phi}{\left[1 - \dfrac{4L\rho}{(L + \rho)^2 + z'^2}\sin^2\phi\right]^{3/2}}$$

$$= \frac{\mu_0 I}{2\pi\,[(L + \rho)^2 + z'^2]^{\frac{1}{2}}} \int \frac{\left[1 + \dfrac{L^2 - \rho^2 - z'^2}{(L + \rho)^2 + z'^2} - k^2\sin^2\phi\right] d\phi}{[1 - k^2\sin^2\phi\ ]^{3/2}}$$

where

$$k^2 = \frac{4L\rho}{(L + \rho)^2 + z'^2} . \tag{2.2}$$

Hence,

$$B_z = \frac{\mu_0 I}{2\pi\,[(L + \rho)^2 + z'^2]^{\frac{1}{2}}}\left[\int \frac{d\phi}{(1 - k^2 \sin^2\phi)^{\frac{1}{2}}} . \right.$$

$$\left. + \frac{L^2 - \rho^2 - z'^2}{(L + \rho)^2 + z'^2} \int \frac{d\phi}{(1 - k^2 \sin^2\phi)^{3/2}}\right] \tag{2.3}$$

The first integral of (2.3) is just the incomplete elliptic integral of the first kind of modulus k, $F(\phi,k)$. To evaluate the second integral of $(2.3)^2$, we write it as

$$\int \frac{d\phi}{(1 - k^2 \sin^2\phi)^{3/2}} = \frac{1}{1 - k^2} \int \frac{(1 - k^2)\, d\phi}{(1 - k^2 \sin^2\phi)^{3/2}}$$

$$= \frac{1}{1 - k^2}\left[\int \frac{(1 - k^2 \sin^2\phi)\, d\phi}{(1 - k^2 \sin^2\phi)^{3/2}} - \int \frac{k^2 \cos^2\phi\, d\phi}{(1 - k^2 \sin^2\phi)^{3/2}}\right] \tag{2.4}$$

The first integral of (2.4) is again the incomplete elliptic integral of the first kind, $F(\phi,k)$. We need to evaluate the second integral of (2.4) This can be accomplished by rewriting it as

$$\int \frac{k^2 \cos^2\phi\, d\phi}{(1 - k^2 \sin^2\phi)^{3/2}} = \int \frac{k^2 \cos\phi\ \ d(\sin\phi)}{(1 - k^2 \sin^2\phi)^{3/2}} ,$$

and then performing an integration by parts. Let

$$u = k^2 \cos\phi ,$$

and

$$dv = \frac{d(\sin\phi)}{(1 - k^2 \sin^2\phi)^{3/2}} .$$

Then $du = -k^2 \sin\phi d\phi$ and it can easily be shown that

$$v = \frac{\sin\phi}{(1 - k^2 \sin^2\phi)^{\frac{1}{2}}} .$$

Hence,

$$\int \frac{k^2 \cos^2\phi \, d\phi}{(1 - k^2 \sin^2\phi)^{3/2}} = \frac{k^2 \sin\phi \cos\phi}{(1 - k^2 \sin^2\phi)^{\frac{1}{2}}} - \int \frac{-k^2 \sin^2\phi \, d\phi}{(1 - k^2 \sin^2\phi)^{\frac{1}{2}}}$$

$$= \frac{k^2 \sin\phi\cos\phi}{(1 - k^2 \sin^2\phi)^{\frac{1}{2}}} - \int (1 - k^2 \sin^2\phi)^{\frac{1}{2}} d\phi + \int \frac{d\phi}{(1 - k^2\sin^2\phi)^{\frac{1}{2}}} . \tag{2.5}$$

The first integral on the right of (2.5) is the incomplete elliptic integral of the second kind of modulus k, $E(\phi,k)$, and again the second integral is $F(\phi,k)$. Combining equations (2.4) and (2.5) gives

$$\int \frac{d\phi}{(1 - k^2 \sin^2\phi)^{3/2}} = \frac{1}{1 - k^2} \left[E(\phi,k) - \frac{k^2 \cos\phi \sin\phi}{(1 - k^2 \sin^2\phi)^{\frac{1}{2}}} \right] . \tag{2.6}$$

Using our expression for k^2 (equation(2.2)), we can show that,

$$\frac{1}{1 - k^2} = \frac{(L + \rho)^2 + z'^2}{(L - \rho)^2 + z'^2} .$$

Then substitution of equation (2.6) into equation (2.3) finally gives us our result:

$$B_z = \frac{\mu_0 I}{2\pi[(L+\rho)^2+z'^2]^{\frac{1}{2}}} \left[F(\phi,k) + \frac{L^2 - \rho^2 - z'^2}{(L-\rho)^2+z'^2} \left\{ E(\phi,k) - \frac{k^2\sin\phi\cos\phi}{(1-k^2\sin^2\phi)^{\frac{1}{2}}} \right\} \right] \Bigg|_{\phi=\phi_1}^{\phi=\phi_2} \tag{2.7}$$

For the purpose of evaluating the above expression at the two limits, the following properties of elliptic integrals are useful:[3]

$$F(-\phi,k) = -F(\phi,k) \ , \tag{2.8}$$

$$E(-\phi,k) = -E(\phi,k) \ , \tag{2.9}$$

$$F(n\pi \pm \phi,k) = 2nK(k) \pm F(\phi,k) \ , \tag{2.10}$$

$$E(n\pi \pm \phi,k) = 2nE(k) \pm E(\phi,k) \ , \tag{2.11}$$

where $K(k) = F(\frac{\pi}{2},k)$ and $E(k) = E(\frac{\pi}{2},k)$ are complete elliptic integrals of the first and second kind, respectively.

It is interesting to compare equation (2.7) with the expression one would obtain for the field due to a pair of complete circular loops. Smith gives the magnetic field due to a single circular loop.[1] For a pair of circular loops symmetric about the z = 0 plane, the value obtained by Smith will be doubled. That is,

$$B_{loop} = \frac{2\mu_0 I}{2\pi[(L + \rho)^2 + z'^2]^{\frac{1}{2}}} \left[K(k) + \frac{L^2 - \rho^2 - z'^2}{(L - \rho)^2 + z'^2} E(k)\right] . \tag{2.12}$$

One can easily verify (with the use of equations (2.8)-(2.11)) that equation (2.7) will reduce to equation (2.12) when we let $\phi_1 = \phi_0$ and $\phi_2 = \phi_0 + \pi$ (i.e., $\theta'_1 = \theta_0$ and $\theta'_2 = \theta_0 + 2\pi$).

It is also instructive to evaluate the average field associated with equation (2.7) at some particular ρ-value, defined as

$$\langle B_z \rangle \equiv \frac{1}{2\pi} \int_0^{2\pi} B_z \ d\theta$$

For this purpose, it is useful to use the expression for B_z from equation (2.1) and then switch the order of integration:

$$\langle B_z \rangle = \frac{1}{2\pi} \int_{\theta'_1}^{\theta'_2} d\theta' \; \frac{\mu_0 I}{2\pi} \int_0^{2\pi} \frac{[L^2 - L\rho \cos(\theta' - \theta)]\, d\theta}{[L^2 + \rho^2 + z'^2 - 2L\rho \cos(\theta' - \theta)]^{3/2}}$$

The integration over θ will proceed in exactly the same way as the integration over θ' proceeded before. However, with the new limits on this integration, $\langle B_z \rangle$ can easily be seen to reduce to

$$\langle B_z \rangle = \left(\frac{\theta'_2 - \theta'_1}{2\pi} \right) \frac{2\mu_0 I}{2\pi [(L + \rho)^2 + z'^2]^{\frac{1}{2}}} \left[K(k) + \frac{L^2 - \rho^2 - z'^2}{(L - \rho)^2 + z'^2} E(k) \right] . \tag{2.13}$$

This well known, but nevertheless interesting, result tells us that the average field due to a pair of circular arcs is just the field we would get from a pair of complete circular loops multiplied by the ratio of the arc length to the circumference of a complete circle.

2.3 Sample Problem

As an example, equation (2.7) will be used to find the median plane magnetic field for a sample problem The geometry of the problem to be considered consists of three pairs of circular arcs (see Figure 2-2). For each pair, the circular arcs are at $z = \pm 1.0$ inch. All three pairs have $L = 15.0$ inch and an angular spread of 46^0. One pair is bisected by $\theta = 0^0$, another by $\theta = 120^0$, and the third pair by $\theta = 240^0$. Each circular arc carries a current of 100 amps in the counter-clockwise sense when viewed from above the x-y plane.

The only mathematical difficulties involved in evaluating equation (2.7) are those associated with finding the values of the incomplete elliptic integrals at the two limits. However, most of today's high speed digital computers are equipped with library subroutines for the

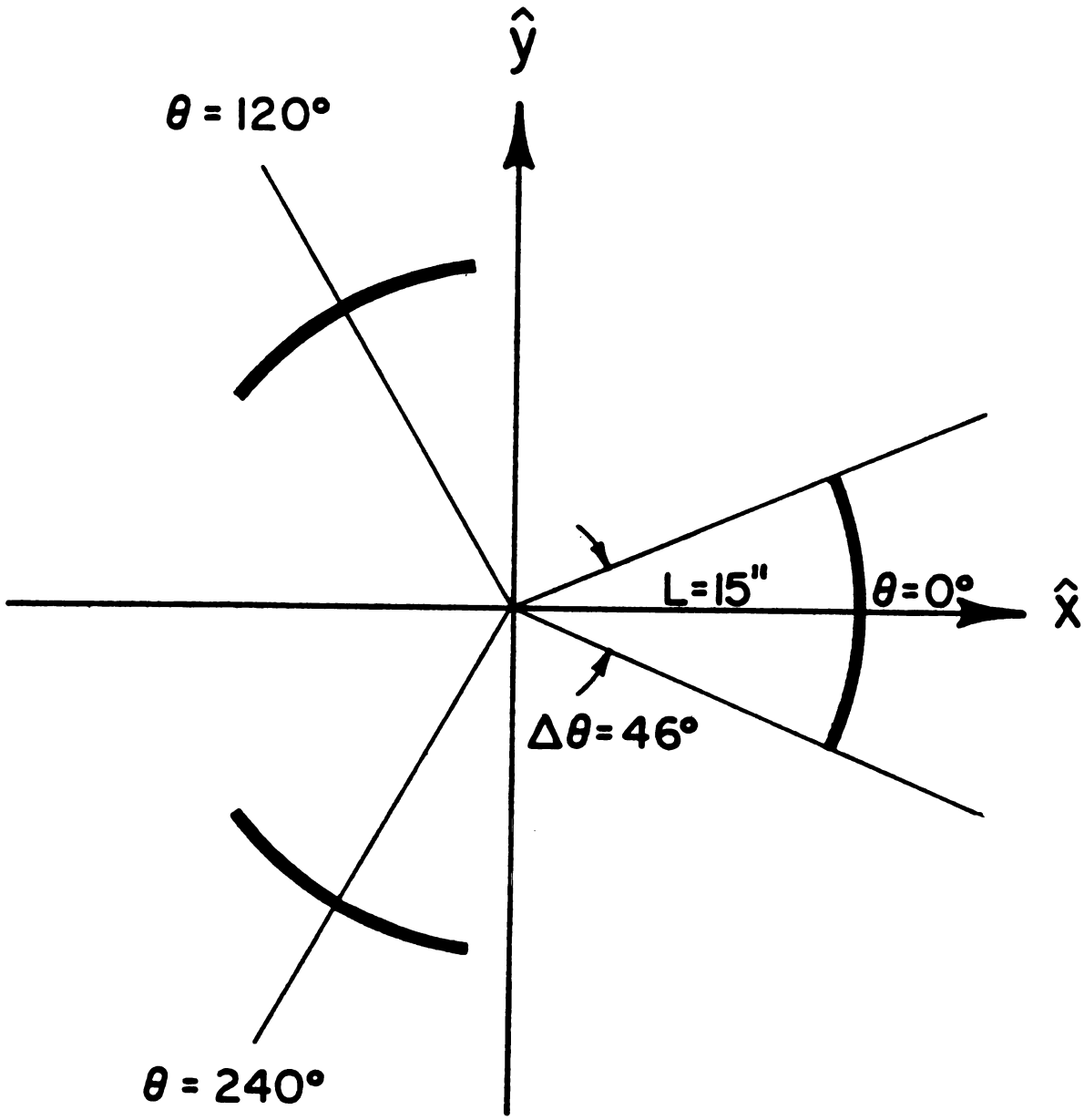

Figure 2-2.--Geometry of the sample problem to be considered. Each circular arc shown actually represents a pair of circular arcs at z = ±1.0 inch. The current, I = 100 amps, is in a counter-clockwise sense.

rapid evaluation of many mathematical functions. In particular, the Michigan State University Cyclotron Laboratory's Xerox Sigma-Seven computer, which was utilized for all computer calculations in this thesis, is equipped with a subset of the IBM Scientific Subroutine package modified for use on the Sigma-Seven.[4] One of these subroutines, ELI2, computes the generalized elliptic integral of the second kind,

$$I = \int_0^{\tan\phi} \frac{A + Bt^2}{\left[(1 + t^2)(1 + k'^2t^2)\right]^{\frac{1}{2}} (1 + t^2)} \, dt \, ,$$

where k' is the complimentary modulus equal to $(1 - k^2)^{\frac{1}{2}}$ and ϕ is the usual argument of the elliptic integrals (i.e., $F(\phi,k)$ or $E(\phi,k)$) and here is assumed to be between $-\pi/2$ and $+\pi/2$. By letting $A = B = 1$, we get the elliptic integral of the first kind and by letting $A = 1$ and $B = k'^2$ we get the elliptic integral of the second kind. (The integrals can be put in a more standard form by letting $k'^2 = 1 - k^2$ and $t = \tan\phi$.)

The method of evaluation used by ELI2 is called Landen's transformation, which allows one to represent elliptic integrals as very rapidly converging infinite products. Descriptions of Landen's transformation and the recurrence relations needed for the evaluation of incomplete elliptic integrals of the first and second kind can be found in a number of different sources.[5,6]

In order to check the accuracy of ELI2, it was used to construct tables of incomplete elliptic integrals of both the first and second kind and these were then compared with standard tables.[5] When all calculations were done with single precision variables, ELI2 was found to give values for elliptic integrals accurate to six significant figures.

Subroutine ELI2 was used in evaluating the necessary elliptic integrals for the sample problem being considered. Since ELI2 assumes

$-\pi/2 \leq \phi \leq +\pi/2$, it was often necessary to make use of the relations (2.8)-(2.11) for the cases when ϕ was outside this range. Using equation (2.7), B_z was calculated for a grid of (ρ,θ) points with ρ extending from 0.0 inch to 37.0 inch with $\Delta\rho = 0.5$ inch, and with $\Delta\theta = 1^o$. Because of the three-fold symmetry of this problem, it was only necessary to calculate B_z for $\theta = 0^o$ to $\theta = 119^o$ and then use $B_z(\rho,\theta + 120^o) = B_z(\rho,\theta + 240^o) = B(\rho,\theta)$, $(0^o \leq \theta < 120^o)$ to obtain the field for $\theta = 120^o$ to $\theta = 359^o$.

A two-dimensional plot of the resulting B-field is shown in Figure 2-3. The equi-B-field contours extend from -6.5 gauss to +8.5 gauss in 0.5 gauss steps. The -6.0, -3.0, 0.0, +3.0 and +6.0 gauss field lines in the vicinity of $\theta = 240^o$ are pointed out explicitly in the figure.

Rather than listing the field values themselves, it is perhaps more enlightening to perform a Fourier analysis of the field and give a list of the Fourier coefficients at each radius value. If we choose $\theta = 0^o$, as in Figure 2-3, then B_z will be an even function of θ and all the sine coefficients will vanish. Also, because of the three-fold symmetry of this problem, we will only get non-vanishing cosine coefficients for harmonic numbers that are multiples of three (i.e., 0, 3, 6, 9...). Table 2.1 lists the Fourier decomposition of the field at some of the radius values at which the field was evaluated. Notice that the second column is actually the average field rather than the zeroth harmonic coefficient B_0 (they are, of course, related by $\langle B_z \rangle = 1/2\, B_0$).

The average B-field from Table 2-1 should be compared with the values we would obtain from the expression for $\langle B_z \rangle$ derived in Section 2.2 (equation (2.9)). This expression can be rewritten as

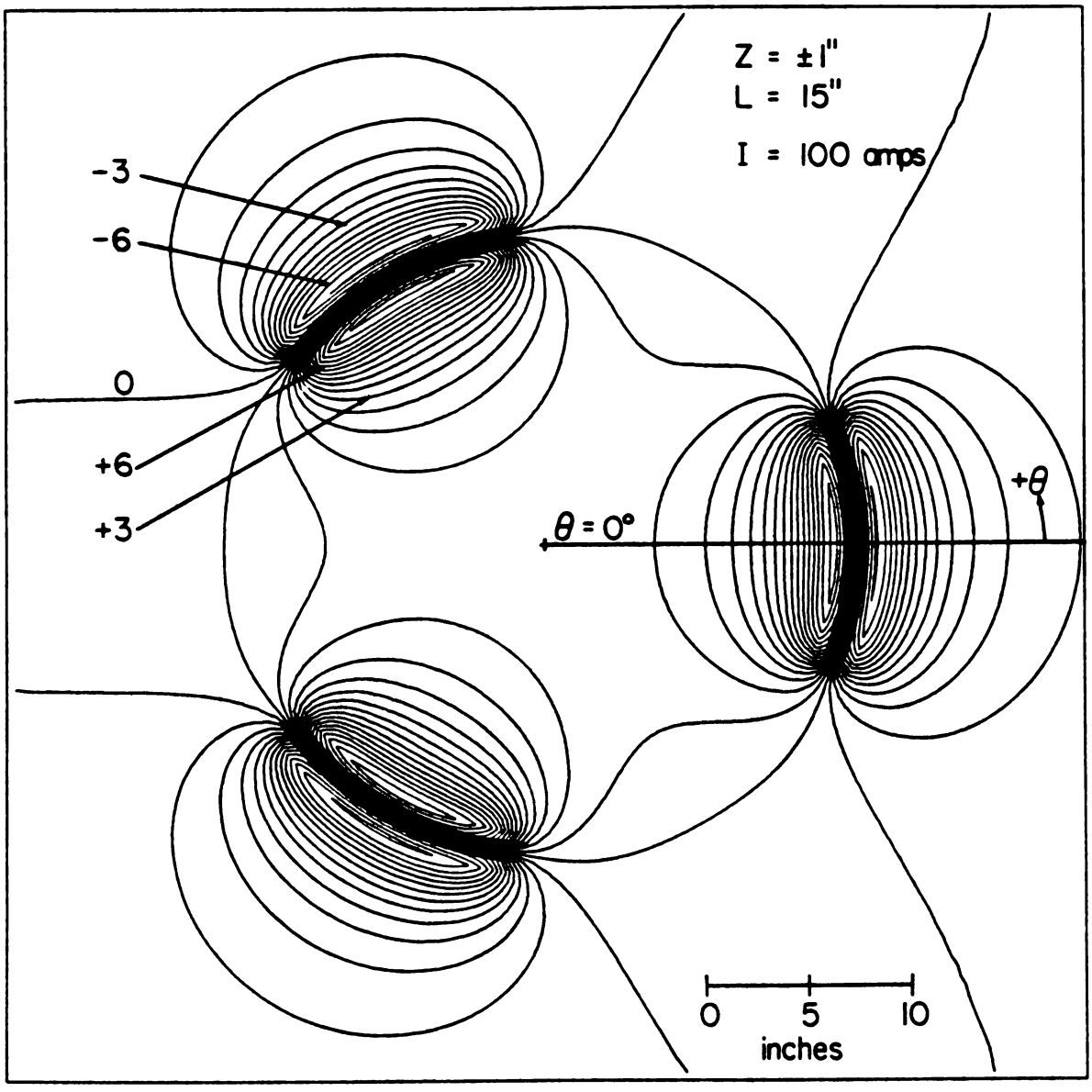

Figure 2-3.--Equi-B-field contours for the median plane magnetic field of the sample problem being considered. The contours extend from -6.5 gauss to +8.5 gauss in 0.5 gauss steps.

Table 2.1.--Fourier decomposition of the median plane magnetic field for the sample problem being considered. Radius is in inches and $\langle B_z \rangle$, B_3, B_6, etc., are given in gauss.

ρ	$\langle B_z \rangle$	B_3	B_6	B_9	B_{12}	B_{15}	B_{18}	B_{21}
.0	1.25595	.00000	.00000	.00000	.00000	.00000	.00000	.00000
2.0	1.27252	.00574	.00001	.00000	.00000	.00000	.00000	.00000
4.0	1.32560	.04752	.00040	.00000	.00000	.00000	.00000	.00000
6.0	1.42728	.17074	.00482	-.00016	-.00002	.00000	.00000	.00000
8.0	1.60633	.44720	.02951	-.00231	-.00063	-.00002	.00001	.00000
10.0	1.93394	1.02091	.12868	-.01942	-.01031	-.00068	.00055	.00015
12.0	2.61571	2.26436	.47283	-.11984	-.10758	-.01203	.01664	.00778
12.5	2.89705	2.77753	.64451	-.18238	-.18322	-.02296	.03560	.01866
13.0	3.24030	3.40473	.86953	-.27228	-.30351	-.04227	.07288	.04253
13.5	3.61781	4.10851	1.14124	-.39113	-.47871	-.07333	.13925	.08955
14.0	3.84347	4.60830	1.36920	-.50567	-.66950	-.11120	.22928	.16027
14.5	3.20967	3.81643	1.17592	-.45546	-.63589	-.11173	.24422	.18123
15.0	.76156	.24723	.02678	.00023	.01032	.00313	-.00915	-.00823
15.5	-1.65029	-3.27504	-1.11017	.45240	.65350	.11781	-.26289	-.19854
16.0	-2.25581	-4.04510	-1.30407	.50555	.69424	.11890	-.25196	-.18063
16.5	-2.04708	-3.59810	-1.10043	.40183	.51803	.08314	-.16489	-.11055
17.0	-1.70854	-2.98155	-.86006	.29381	.35316	.05275	-.09725	-.06057
17.5	-1.40989	-2.44864	-.66361	.21136	.23612	.03272	-.05594	-.03228
18.0	-1.17213	-2.02554	-.51457	.15255	.15822	.02033	-.03220	-.01720
20.0	-.62878	-1.05445	-.20562	.04582	.03545	.00339	-.00398	-.00158
22.0	-.38869	-.62456	-.09419	.01601	.00941	.00068	-.00061	-.00018
24.0	-.26242	-.40143	-.04749	.00628	.00286	.00016	-.00011	-.00003
26.0	-.18786	-.27285	-.02571	.00269	.00097	.00004	-.00002	.00000
28.0	-.14024	-.19327	-.01471	.00124	.00036	.00001	-.00001	.00000
30.0	-.10805	-.14136	-.00881	.00060	.00014	.00000	.00000	.00000

$$\langle B_z(\rho)\rangle = \frac{\Delta\theta}{2\pi}\ B_{loop}\ (\rho)\ ,$$

where $\Delta\theta$ represents the total angular spread of the circular arcs for the geometry we are considering and $B_{loop}(\rho)$ is the median plane magnetic field from a pair of complete circular loops at a radius of ρ. For our problem,

$$\frac{\Delta\theta}{2\pi} = \frac{3 \times 46^0}{360^0} = .38333$$

and $B_{loop}(\rho)$ can be calculated from equation (2.12). It was found that $\langle B_z(\rho)\rangle$ calculated from the above expression agrees with the values from Table 2-1 to six significant figures, with an occasional disagreement of one unit in the sixth significant figure.

Finally, whenever one is using a computer to perform long extensive calculations in solving a problem, two important considerations should always be kept in mind: the amount of computer time it takes to arrive at a solution to the problem, and how accurately does our solution represent the real answer to the problem.

It is often advantageous to experiment with alternate approaches to a problem in an effort to cut down on computer run time and/or increase the accuracy of the calculations. For the sample problem we have been considering, one can also use an approximate method for determining the median plane magnetic field which doesn't require the evaluation of any elliptic integrals. This can be a valuable saver in computer run time. The procedure is to consider each of our current carrying circular arcs as being composed of several short line segments connected end to end. The z-component of the field due to each one of these short segments can be calculated exactly at all points in the median plane.

Referring to Figure 2-4, if we consider a line segment of length a which is parallel to the x-y plane and located at z = +z', then it can be shown that the field at a point (x,y) is given by

$$B_{z\text{-wire}}(x,y) = \frac{\mu_0 I}{4\pi\,(x'^2 + z'^2)^{\frac{1}{2}}} \left[\frac{y' - a}{(x'^2 + z'^2 + (y' - a)^2)^{\frac{1}{2}}} - \frac{y'}{(x'^2 + z'^2 + y'^2)^{\frac{1}{2}}} \right] , \tag{2.14}$$

where

$$x' = (x - x_1)\cos\theta + (y - y_1)\sin\theta \quad , \tag{2.15}$$

and

$$y' = -(x - x_1)\sin\theta + (y - y_1)\cos\theta \quad . \tag{2.16}$$

Here, (x_1, y_1) locates an endpoint of the wire and θ represents the angle the wire makes with the positive y-axis when rotated counter-clockwise about (x_1, y_1). A summation over all the line segments making up a circular arc will give us the approximate median plane magnetic field due to that arc, and, finally, a summation over all three pairs of arcs will give us an approximate solution to our problem.

The accuracy of this method obviously increases with the number of line segments we divide our circular arcs into, but so does the computer run time. Therefore, a comparison of computer time and accuracy was made between the evaluation of the exact expression for B_z, equation (2.7) and the approximate method described above.

For the approximate method, a computer program named WIRE FIELD was used[7] (with slight modifications for print-out purposes). WIRE FIELD uses the expressions (2.14)-(2.16) in calculating the median plane magnetic field. If a θ-symmetry exists in the problem being solved with WIRE FIELD, the user indicates this by inputting the number of sectors for which the field will be identical. (For our sample problem there are three sectors.) The wire segments making up a circular

Figure 2-4.--Geometry to be considered when calculating the field due to a line segment. The wire has length $\underline{a}$, and is located at $z = +z'$. The current, I, flows in the positive $\hat{y}'$ direction. The field is first calculated in the primed system and then a transformation is made to the unprimed system (see equations (14)-(16)).

Figure 2-5.--Relation between the radius of a circle, r, and the location of a straight line segment, r', subtending the same angle such that the arc length equals the segment length.

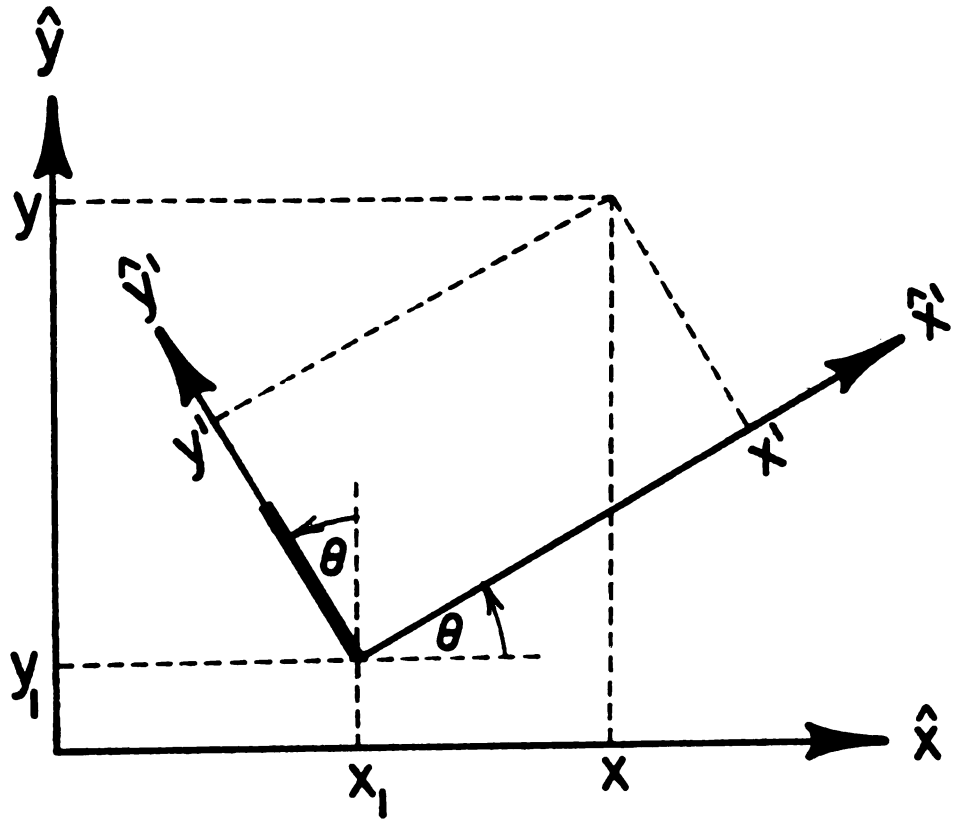

Figure 2-4

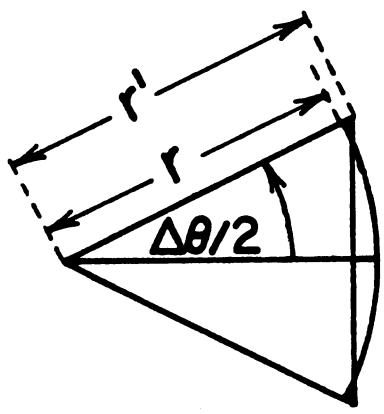

$$r\,(\Delta\theta/2) = r'\sin(\Delta\theta/2)$$

Figure 2-5

arc in one sector are specified by giving their endpoints in polar coordinates, (r_1,θ_1) and (r_2,θ_2), their height above the median plane z', and their current I. The program will assume a duplicate wire at z = -z' and also a duplicate pair of wires in each sector.

Circular arcs divided into 1, 2, 4, 8, and 16 segments were studied. (That is, straight line currents were used to approximate arcs of $\Delta\theta = 46^0$, 23^0, 11.5^0, 5.75^0, and 2.875^0, respectively. The r-value for the location of the endpoints of the straight line segments was adjusted in each case so that the segmented arc had the same total length as the circular arc. The appropriate relation (see Figure 2-5)is given by

$$r' = r \frac{(\Delta\theta/2)}{\sin(\Delta\theta/2)} ,$$

where r is the radius of the circular arc and $\Delta\theta$ is the angle subtended by the arc that the straight line segment is approximating.

Table 2.2 compares the median plane magnetic field obtained from the exact equation and the segmented cases. The values listed are along a radial line that bisects one of the circular arc pairs (i.e.,$\theta = 0^0$). This is where we expect the most significant differences to occur. The values listed under the exact case are accurate to at least five significant figures. The numbers in parentheses under the column headings represent the approximate computer execution times in minutes to calculate the field at a grid of 120 x 75 points and to write this field to the line printer and also to a magnetic disc for permanent storage.

From Table 2.2, we see that the biggest differences between the exact case and the segmented cases occurs in the vicinity of the arcs (≈15.0 inch). For the 16 segment case, this amounts to only 0.026 gauss difference, but this case took 1.4 times more computer time to run.

Table 2.2.--Median plane magnetic field along $\theta = 0^0$ for the sample problem being considered. This table compares B_z for the exact case with five different segmented cases (see text). The numbers in parentheses indicate computer run times in minutes. Radius is in inches and fields are in gauss.

ρ	Exact	16	8	4	2	1
	(6.63)	(9.18)	(4.95)	(2.83)	(1.75)	(1.23)
.0	1.25595	1.25608	1.25647	1.25804	1.26445	1.29216
2.0	1.27826	1.27840	1.27880	1.28043	1.28708	1.31602
4.0	1.37352	1.37367	1.37412	1.37594	1.38342	1.41691
6.0	1.60266	1.60285	1.60339	1.60563	1.61498	1.66018
8.0	2.08008	2.08034	2.08114	2.08439	2.09838	2.17653
10.0	3.05381	3.05432	3.05586	3.06221	3.08977	3.28150
12.0	5.13501	5.13645	5.14071	5.15824	5.22734	5.85985
12.5	5.97664	5.97850	5.98411	6.00708	6.09369	6.88433
13.0	6.99019	6.99252	6.99943	7.02826	7.13454	7.81647
13.5	8.10088	8.10306	8.10962	8.14138	8.27224	7.48812
14.0	8.81974	8.81879	8.81701	8.84207	9.03796	3.06168
14.5	7.29722	7.28416	7.25460	7.27116	7.72342	-4.17398
15.0	1.03873	1.01320	.96060	.99438	1.80428	-7.28418
15.5	-5.13125	-5.14377	-5.17004	-5.13992	-4.62534	-7.07209
16.0	-6.59761	-6.59845	-6.59918	-6.56881	-6.36619	-6.05808
16.5	-5.94994	-5.94794	-5.94177	-5.91160	-5.80330	-5.06093
17.0	-4.97445	-4.97240	-4.96627	-4.94124	-4.86502	-4.23126
17.5	-4.11399	-4.11238	-4.10760	-4.08863	-4.03111	-3.56399
18.0	-3.42282	-3.42164	-3.41813	-3.40424	-3.36064	-3.02801
20.0	-1.80931	-1.80898	-1.80799	-1.80407	-1.79017	-1.70271
22.0	-1.08209	-1.08199	-1.08169	-1.08049	-1.07606	-1.05045
24.0	-.70217	-.70214	-.70205	-.70168	-.70032	-.69270
26.0	-.48275	-.48274	-.48272	-.48263	-.48232	-.48048
28.0	-.34662	-.34662	-.34662	-.34662	-.34666	-.34674
30.0	-.25747	-.25747	-.25748	-.25751	-.25766	-.25831

In the four segment case, we have a maximum difference of 0.044 gauss, but this case ran 2.3 times faster than the exact case.

The conclusion to be reached on the basis of this short study is that if one wants more than a few percent accuracy, then the exact equation using elliptic integrals is the route to proceed. For the cases when the circular arcs are divided into approximately 12 or more segments, the segmented cases take more computer time to run without the equivalent accuracy.

3. A SOURCE TO PULLER PROGRAM FOR THE CALCULATION OF ION TRAJECTORIES

3.1 Introduction

In the ion-source to puller electrode region of a cyclotron, there are many problems concerning the acceleration of ions that warrant study. Some of these include the energy gain in the first acceleration gap, the ion's transit time across the gap, and the effects that a D.C. extraction grid placed in front of the ion-source has on the ions. A nice feature concerning these problems is that they can be studied independently of the particle's orbit through the rest of the cyclotron. Therefore, a computer program, called TRAJECTORY, was written for the calculation of ion trajectories in the source to puller region alone. The program assumes a homogeneous magnetic field and uses measured or simulated potential maps for determining the electric fields.

Descriptions of the relevant equations used in TRAJECTORY, the numerical integration employed, the computation of fields and potentials, and input-output features, are contained in Section 3.2. The reliability of TRAJECTORY is tested in Section 3.3 where its predictions are compared with a case which can be solved analytically and also with predictions from the orbit code CYCLONE.

Finally, in Section 3.4, TRAJECTORY will be used to study some of the previously mentioned problems. In particular, the energy gain and transit time across the first acceleration gap for several different ions will be studied.

3.2 Description of the TRAJECTORY Program

TRAJECTORY is a program for the calculation of charged particle trajectories in the source to puller region of a cyclotron. It considers only motion in the z = 0 plane and calculates the trajectories of particles subject to the forces of crossed electric and magnetic fields. Many of the techniques used in this program have been adapted from another particle orbit code in use at Michigan State University's Cyclotron Lab[8], and will be described in the sections which follow.

3.2.1 Equations

The relativistically correct equations of motion for a particle of charge q can be written simply as,

$$\frac{d\vec{p}}{dt} = q(\vec{E} + \vec{v} \times \vec{B}) \ , \qquad (3.1)$$

where $\vec{p} = m\vec{v} = \gamma m_0 \vec{v}$, m_0 being the particle rest mass and $\gamma = (1 - v^2/c^2)^{-\frac{1}{2}}$ the relativistic gamma factor. If one employs what are known as "cyclotron units,"[2,8] then equation (3.1) can be put in a form more suitable for cyclotron work.

The cyclotron units include the B-field unit B_0, the frequency unit ω_0, and the length unit a. B_0, usually given in kG, is used to define $\omega_0 (=2\pi\nu_0)$ which is the cyclotron frequency for a particle of charge q and rest mass m_0:

$$\omega_0 = \frac{qB_0}{m_0}$$

The cyclotron radio frequency, ω_{RF}, is related to ω_0 by,

$$\omega_{RF} = h(1 + \varepsilon)\omega_0$$

where h is the harmonic number and ε represents a frequency error. The length unit is taken as the radius at which a particle moving with the speed of light would travel if rotating at a frequency ω_0. That is,

$$a = \frac{c}{\omega_0} ,$$

and it can be shown that the length unit in inches is given by,

$$a(\text{in.}) = \frac{1000 \times m_0c^2(\text{MeV})}{(q/e) \times B_0(\text{kG}) \times 299.7925 \times 2.54} .$$

It is also convenient to represent momenta in units of inches. This is accomplished by dividing all momenta by m_0c and multiplying by the length unit a, or equivalently,

$$\left(\frac{\vec{p}}{m_0c}\right) a = \frac{\vec{p}}{m_0\omega_0} .$$

Rather than using real time, t, as our independent variable in equation (3.1), we use a dimensionless quantity $\tau = \omega_{RF}t$ called the R.F. time. With the above changes and employing the cyclotron units, equation (3.1) can be written as,

$$\frac{d}{d\tau}\left(\frac{\vec{p}}{m_0\omega_0}\right) = \frac{q}{m_0\omega_0\omega_{RF}}\left(E + \frac{\vec{p}}{\gamma m_0} \times \vec{B}\right) ,$$

or, after a little algebra,

$$\frac{d}{d\tau}\left(\frac{\vec{p}}{m_0\omega_0}\right) = \frac{a^2}{h(1+\varepsilon)}\ \frac{q}{m_0c^2}\ \vec{E} + \frac{1}{h(1+\varepsilon)\gamma}\left(\frac{\vec{p}}{m_0\omega_0}\right) \times \left(\frac{\vec{B}}{B_0}\right) \quad (3.2)$$

The left hand side of (3.2) has units of inches. If q is given in units of the electron charge e, $\vec{E}$ in $\frac{MV}{inch}$ and m_0c^2 in MeV, then the first term on the right of (3.2) is also seen to be in inches. Since $(\vec{B}/B_0)$

is a dimensionless quantity, the second term on the right also has units of inches. For convenience of notation, the momentum in inches will hereafter be written as,

$$P(\text{in.}) = \frac{\vec{p}}{m_0\omega_0} \quad .$$

The present program assumes a uniform magnetic field given by $\vec{B} = -B_0\hat{z}$. This allows the program to run much quicker than if a grid of B-field points was input since no interpolation is necessary. The justification for the uniform field is that $\vec{B}$ will vary very little over the small source to puller region where this program will be utilized.

Since motion is only considered in the z = 0 plane, we have $\vec{P} = P_x\,\hat{x} + P_y\,\hat{y}$, and $\vec{E} = E_x\hat{x} + E_y\,\hat{y}$. Hence, from (3.2) we then obtain the equations of motion in cartesian coordinates which is the form used by TRAJECTORY:

$$\frac{dP_x}{d\tau} = \frac{a^2}{h(1+\varepsilon)}\,\frac{q}{m_0c^2}\,E_x - \frac{1}{h(1+\varepsilon)\gamma}\,P_y \quad , \tag{3.3}$$

$$\frac{dP_y}{d\tau} = \frac{a^2}{h(1+\varepsilon)}\,\frac{q}{m_0c^2}\,E_y + \frac{1}{h(1+\varepsilon)\gamma}\,P_x \quad . \tag{3.4}$$

It is also easy to see that,

$$\frac{dx}{d\tau} = \frac{1}{h(1+\varepsilon)\gamma}\,P_x \quad , \tag{3.5}$$

$$\frac{dy}{d\tau} = \frac{1}{h(1+\varepsilon)\gamma}\,P_y \quad . \tag{3.6}$$

A particle's energy in TRAJECTORY is calculated in two different fashions. One method uses the particle's momentum, and it can be shown that the usual relation

$$E_{kin} = \sqrt{m_0^2c^4 + p^2c^2} - m_0c^2 \ ,$$

can be put in the form

$$E_{kin} = m_0c^2 \frac{P^2/a^2}{\sqrt{1 + P^2/a^2} + 1} \tag{3.7}$$

where P is again the momentum in inches and $\underline{a}$ is the length unit also in inches. Since $P^2 = P_x^2 + P_y^2$ and P_x and P_y are obtained by solving the equations of motion, this means that we needed to calculate the electric fields in determining E_{kin}. And since computing the electric fields involves taking derivatives of potentials, a small fluctuation in the potential data may have a pronounced effect on the kinetic energy calculated from equation (3.7).

It is therefore desirable to calculate kinetic energy by an alternate method which uses only the potential data, and not the associated fields. This then represents the second method by which a particle's energy is calculated in TRAJECTORY. This method involves what is know as the "J-equation",[2] and it is fairly easy to show how it comes about.

The kinetic energy of a particle can be written as

$$E = (\gamma - 1)m_0c^2 \ ,$$

so that

$$\frac{dE}{dt} = \frac{d}{dt}(\gamma m_0c^2) = \gamma^3 m_0 v \frac{dv}{dt} \ . \tag{3.8}$$

In the last step $\frac{d\gamma}{dt} = \gamma^3 \frac{v}{c^2} \frac{dv}{dt}$ was used. We also have the equations of motion

$$\frac{d(\gamma m_0 \vec{v})}{dt} = q(\vec{E} + \vec{v} \times \vec{B}) \ .$$

If we take the dot product of $\vec{v}$ and the above equation we obtain

$$\vec{v} \cdot \frac{d(\gamma m_0 \vec{v})}{dt} = q\vec{v} \cdot \vec{E} \ . \tag{3.9}$$

Working with the left hand side of (3.9),

$$\vec{v} \cdot \frac{d(\gamma m_0 \vec{v})}{dt} = m_0 \vec{v} \cdot \left(\vec{v} \frac{d\gamma}{dt} + \gamma \frac{d\vec{v}}{dt} \right)$$

$$= \gamma m_0 v \frac{dv}{dt} \left(\frac{v^2}{c^2} \gamma^2 + 1 \right)$$

$$= \gamma^3 m_0 v \frac{dv}{dt} \ . \tag{3.10}$$

Hence, combining (3.8)-(3.10) we obtain

$$\frac{dE}{dt} = q\vec{v} \cdot \vec{E} \ . \tag{3.11}$$

If the potential is given by $V = V(x,y,t)$, then

$$\frac{dV}{dt} = \frac{\partial V}{\partial t} + \frac{\partial V}{\partial x} \frac{dx}{dt} + \frac{\partial V}{\partial y} \frac{dy}{dt}$$

$$= \frac{\partial V}{\partial t} - \vec{E} \cdot \vec{v} \tag{3.12}$$

Using (3.12), (3.11) becomes,

$$\frac{dE}{dt} = q\left(\frac{\partial V}{\partial t} - \frac{dV}{dt} \right) \ ,$$

or if we put all the total derivatives on the left hand side, and divide through my ω_{RF} we get our result:

$$\frac{dJ}{d\tau} = q \frac{\partial V(x,y,\tau)}{\partial \tau} \tag{3.13}$$

where

$$J = E_J + qV(x,y,\tau) \ . \tag{3.14}$$

The J-equation, (3.13), is just another relation that can be numerically integrated right along with the equations of motion. Once J is found then the kinetic energy can be obtained simply from (3.14). Comparing the energy from the J-equation with the energy obtained from equation (3.7) will give us some idea of the "noise" in the potential data.

3.2.2 Runga-Kutta Integration

The equations of motion, (3.3)-(3.6), and the J-equation, (3.13), are numerically integrated in TRAJECTORY via a fourth order Runga-Kutta routine.[9] The independent variable is τ and the integration step size in the Runga-Kutta process has normally been taken as one R.F. degree. This has been found to allow the program to run quickly and with considerable accuracy.

3.2.3 Fields and Potentials

TRAJECTORY allows the user to input two separate potential maps from which the electric fields are derived. One map corresponds to the spatial part of the normal radio frequency field, and the second map (if used) corresponds to a D.C. field. Hence, the potential at some point (x,y) and at a R.F. time τ, will be given by

$$V(x,y,\tau) = V_{DC}(x,y) + V_{RF}(x,y)\cos\tau \qquad (3.15)$$

The potential maps consist of rectangular arrays of equally spaced potential values. These maps are usually obtained through electrolytic tank or conducting paper measurements, but can also, of course, be found by other means, such as relaxation.

Fields and potentials at locations lying between the given potential points are obtained through a double-weighted three-point Lagrange

interpolation.[8] The advantage of a weighted three point interpolation over a straight three or four point interpolation is that with this method the fields as well as the potentials will be continuous.

The procedure actually uses four points in each interpolation. For example, suppose V_1, V_2, V_3, and V_4 are the potentials at four equally spaced points x_1, x_2, x_3, and x_4 respectively, and we wish to find the potential at $x_2 + fs$ where f is a fractional distance between x_2 and x_3 and s is the spacing between the points. Then, using a standard three-point Lagrange interpolation,[10] we fit a parabola to V_1, V_2, and V_3 to find the potential at $x_2 + fs$:

$$V'(x_2 + fs) = \frac{f(f - 1)}{2} V_1 + (1 - f^2)V_2 + \frac{f(f + 1)}{2} V_3 ,$$

and it is easy to show that a three-point Lagrange interpolation using V_2, V_3, and V_4 also gives for the potential at $x_2 + fs$:

$$V''(x_2 + fs) = \frac{(1 - f)(2 - f)}{2} V_2 + f(2 - f)V_3 + \frac{f(f - 1)}{2} V_4$$

Now, we take a weighted average between V' and V'' to get a value for $V(x_2 + fs)$:

$$V(x_2 + fs) = (1 - f)V'(x_2 + fs) + fV''(x_2 + fs) ,$$

which can be written as,

$$V(x_2 + fs) = \sum_{i=1}^{4} c_i(f)V_i$$

where a little algebra shows that the $c_i(f)$ are given by,

$$\left.\begin{aligned} c_1 &= f^2 - \tfrac{1}{2}(f^3 + f) \\ c_2 &= \tfrac{3}{2}f^3 - \tfrac{5}{2}f^2 + 1 \\ c_3 &= 2f^2 - \tfrac{3}{2}f^3 + \tfrac{1}{2}f \\ c_4 &= \tfrac{1}{2}(f^3 - f^2) \end{aligned}\right\} \quad (3.16)$$

The field at $x_2 + fs$ is given by $E_x = -\frac{\partial V}{\partial x} = -\frac{\partial V}{\partial f}\frac{\partial f}{\partial x}$, so that,

$$E_x(x_2 + fs) = -\sum_{i=1}^{4} c_{i+4}(f)\, V_i / s$$

where c_5, c_6, c_7, and c_8 are just the derivatives with respect to f of c_1, c_2, c_3, and c_4, respectively. That is,

$$\left.\begin{aligned} c_5 &= 2f - \tfrac{3}{2}f^2 - \tfrac{1}{2} \\ c_6 &= \tfrac{9}{2}f^2 - 5f \\ c_7 &= 4f - \tfrac{9}{2}f^2 + \tfrac{1}{2} \\ c_8 &= \tfrac{3}{2}f^2 - f \end{aligned}\right\} \quad (3.17)$$

The above example has been in one-dimension. The extension to two-dimension is simple:

$$V(x_2 + f_x s, y_2 + f_y s) = \sum_{i=1}^{4}\sum_{j=1}^{4} c_i(f_x)\, c_j(f_y)\, V_{ij}$$

$$E_x(x_2 + f_x s, y_2 + f_y s) = \sum_{i=1}^{4}\sum_{j=1}^{4} c_{i+4}(f_x)\, c_j(f_y)\, V_{ij} / s$$

$$E_y(x_2 + f_x s, y_2 + f_y s) = \sum_{i=1}^{4}\sum_{j=1}^{4} c_i(f_x)\, c_{j+4}(f_y)\, V_{ij} / s$$

Hence, in the two dimensional case, the potential and fields at any given point involve the potentials of a 4 x 4 grid of the input data.

3.2.4 Input-Output Features

The potential data, along with its identification and relevant geometrical data, is stored in a file on a magnetic disc from which the program will read it. All other parameters are input via computer cards. These include the particle's rest mass m_0c^2 and charge q/e, the field unit B_0, the R.F. starting time τ_0, the initial kinetic energy E_0, the

frequency error ε, the harmonic number h, the voltages for the D.C. and R.F. fields, and the initial position and direction of the particle relative to the source slit. The program will automatically calculate the R.F. frequency ν_{RF}, but as an option the user may input a specific value for this.

The output consists of the particle's position, momentum, and energy as a function of the RF time τ, and the fields and potentials at the position of the particle.

The equations of motion are integrated until the particle reaches the edge of the potential field or until it has spent a certain maximum allowable time in the field.

3.3 Reliability of TRAJECTORY

As a check on the reliability of TRAJECTORY, its predicted orbit for a few selected cases was compared with the orbits obtained by other means. In particular, it was compared with (1) a case for which a completely analytic solution can be obtained, and (2) another orbit code called CYCLONE.

3.3.1 Comparison with Analytic Solution

A case for which a completely analytic solution can be obtained is that of the non-relativistic approximation to the acceleration of an ion through spatially uniform electric and magnetic fields. This means that we assume the magnetic field is given just as before by $\vec{B} = -B_0\hat{z}$ and for the electric field we will assume the form

$$E_x = E_1 + E_2 \cos\tau \,, \tag{3.18}$$

$$E_y = E_3 + E_4 \cos\tau \,. \tag{3.19}$$

The non-relativistic approximation means that we let $\gamma = 1$ in equations (3.3)-(3.6). This is a valid approximation if the ions are of sufficiently low energy.

If in equations (3.3)-(3.6) we let

$$A = \frac{a^2}{h(1+\varepsilon)} \frac{q}{m_0 c^2} \quad ,$$

and

$$B = \frac{1}{h(1+\varepsilon)} \quad ,$$

then these equations can be rewritten as (setting $\gamma = 1$)

$$\frac{dP_x}{d\tau} = AE_x - BP_y \quad ,$$

$$\frac{dP_y}{d\tau} = AE_y + BP_x \quad ,$$

$$\frac{dx}{d\tau} = BP_x \quad ,$$

$$\frac{dy}{d\tau} = BP_y \quad .$$

With E_x and E_y given by (3.18) and (3.19), respectively, the above equations can be solved exactly. If we assume the initial conditions $P_x(\tau_0) = P_{x_0}$, $P_y(\tau_0) = P_{y_0}$, $x(\tau_0) = x_0$, and $y(\tau_0) = y_0$, where τ_0 is the initial R.F. time, then the solution of these equations can (painstakingly) be shown to be given by

$$P_x = f_1(\tau) + f_5(\tau) \quad ,$$

$$P_y = f_2(\tau) + f_6(\tau) \quad ,$$

$$x = x_0 + [f_6(\tau) - f_6(\tau_0)] + [f_3(\tau) - f_3(\tau_0)] \quad ,$$

$$y = y_0 + [f_4(\tau) - f_4(\tau_0)] - [f_5(\tau) - f_5(\tau_0)],$$

where for $B \neq 1$ we have

$$f_1(\tau) = \frac{-AE_3}{B} + \frac{A}{1 - B^2} [E_2 \sin(\tau) + BE_4\cos(\tau)] ,$$

$$f_2(\tau) = \frac{AE_1}{B} + \frac{A}{1 - B^2} [E_4 \sin(\tau) - BE_2\cos(\tau)] ,$$

$$f_3(\tau) = -AE_3\tau - \frac{AB}{1 - B^2} [E_2 \cos(\tau) - BE_4\sin(\tau)] ,$$

$$f_4(\tau) = AE_1\tau - \frac{AB}{1 - B^2} [E_4 \cos(\tau) + BE_2\sin(\tau)] ,$$

$$f_5(\tau) = C_1 \cos(B\tau) - C_2\sin(B\tau) ,$$

$$f_6(\tau) = C_1 \sin(B\tau) + C_2\cos(B\tau) ,$$

and

$$C_1 = [P_{x0} - f_1(\tau_0)] \cos(B\tau_0) + [P_{y0} - f_2(\tau_0)] \sin(B\tau_0) ,$$

$$C_2 = -[P_{x0} - f_1(\tau_0)] \sin(B\tau_0) + [P_{y0} - f_2(\tau_0)] \cos(B\tau_0) ,$$

and for $B = 1$ we have

$$f_1(\tau) = -AE_3 + \frac{AE_2}{4} [\sin(\tau) + 2\tau \cos(\tau)] - \frac{AE_4}{4} [\cos(\tau) + 2\tau \sin(\tau)],$$

$$f_2(\tau) = AE_1 + \frac{AE_4}{4} [\sin(\tau) + 2\tau \cos(\tau)] + \frac{AE_2}{4} [\cos(\tau) + 2\tau \sin(\tau)],$$

$$f_3(\tau) = -AE_3\tau + \frac{AE_2}{4} [2\tau\sin(\tau) + \cos(\tau)] - \frac{AE_4}{4} [3\sin(\tau) - 2\tau\cos(\tau)],$$

$$f_4(\tau) = AE_1\tau + \frac{AE_4}{4} [2\tau\sin(\tau) + \cos(\tau)] + \frac{AE_2}{4} [3\sin(\tau) - 2\tau\cos(\tau)],$$

$$f_5(\tau) = C_1 \cos(\tau) - C_2 \sin(\tau),$$

$$f_6(\tau) = C_1 \sin(\tau) + C_2 \cos(\tau),$$

and

$$C_1 = [P_{x0} - f_1(\tau_0)] \cos\tau_0 + [P_{y0} - f_2(\tau_0)] \sin\tau_0 ,$$

$$C_2 = -[P_{x0} - f_1(\tau_0)] \sin\tau_0 + [P_{y0} - f_2(\tau_0)] \cos\tau_0 .$$

A computer program was written employing the above equations and having a similar input and output format to TRAJECTORY for easy comparison.

In TRAJECTORY, a grid of potentials producing a spatially uniform electric field was used. The R.F. voltage was adjusted to give a field equal to the average field that exists in the source to puller region for a measured field (called 1.06.5-A) when 100 kV is placed on the puller. That is, the R.F. voltage was adjusted to give 252.74142 kV/inch. (Field 1.06.5-A will be described in Section 3.4.) The equivalent input for the analytic case was $E_1 = E_2 = E_3 = 0$, and $E_4 = 252.74142$ kV/inch. The magnetic field strength in both cases was taken as 47.8 kG.

The two programs were then compared for the first harmonic acceleration of $^{14}N^{4+}$ ($\nu_{RF} \simeq 20.97$ MHz). This particle was given a small initial energy of 40 eV and was initially directed along the electric field direction. The R.F. starting time was taken as $\tau_0 = -45^\circ$ (45° before peak field).

Table 3.1 compares TRAJECTORY and the analytic solution for some selected points along the orbit. We see that for $\tau = 0^\circ$, the particle energies differ by only 1.0 eV out of $\simeq .15$ MeV. And at $\tau = 45^\circ$, the particle energies differ by only 6.0 eV out of $\simeq .56$ MeV. Differences in particle positions for the two cases can similarly be seen to be very minute.

The agreement here is excellent. The slight disagreement as we

Table 3.1.--Comparison of TRAJECTORY and the analytic solution for the first harmonic acceleration of $^{14}N^{4+}$ through homogeneous magnetic and electric fields.

τ_0	x (in.)		y (in.)		E (MeV)	
	Anayltic	TRAJECTORY	Anayltic	TRAJECTORY	Anayltic	TRAJECTORY
-45^o	.000000	.000000	.000000	.000000	.000040	.000040
-30^o	-.001631	-.001631	.018023	.018023	.014901	.014901
-15^o	-.012529	-.012529	.071317	.071317	.064844	.064844
0^o	-.042116	-.042115	.160461	.160461	.154038	.154039
15^o	-.099285	-.099282	.280815	.280814	.274248	.274249
30^o	-.191046	-.191039	.422743	.422740	.406300	.406303
45^o	-.321312	-.321299	.572360	.572355	.525960	.525966
60^o	-.489934	-.489910	.712774	.712768	.612445	.612455

move to higher particle energies is undoubtedly due to relativistic effects coming into play since the analytic solution ignores these. At E = .56 MeV, we have,

$$\gamma = 1 + \frac{E}{m_0 c^2} = 1 + \frac{.56}{13041.8} = 1.000043$$

Although $\gamma - 1$ is still very small, it is still large enough to produce deviations on the order of those mentioned above.

TRAJECTORY was also compared with the analytic solution for the third harmonic acceleration of $^{14}N^{4+}$. All other initial conditions were the same as those described above. Excellent agreement was again obtained (to the degree mentioned above).

3.3.2 Comparison with CYCLONE

Finally, TRAJECTORY was compared with the orbit code CYCLONE. CYCLONE is a program for calculating orbits in the central region of a cyclotron and has been utilized at Michigan State University for several years. CYCLONE uses a measured (or simulated) potential grid for the calculation of the electric field, and the magnetic field is input via its Fourier coefficients.

The same potential grid (1.06.5-A, described in Section 3.4) was used in both TRAJECTORY and CYCLONE. Both programs used 100 kV maximum voltage on the puller (giving again $\langle \vec{E}_y \rangle$ = 252.74142 kV/inch in the source to puller region). The Fourier coefficients for the magnetic field in CYCLONE were input to produce a uniform field of 47.8 kG, the same field used in TRAJECTORY.

TRAJECTORY and CYCLONE were then used to again study the first harmonic acceleration of $^{14}N^{4+}$. The particle was once again given a

Table 3.2.--Comparison of TRAJECTORY and CYCLONE for the first harmonic acceleration of $^{14}N^{4+}$ through a homogeneous magnetic field and a measured electric field, 1.06.5-A.

τ_0	x (in.)		y (in.)		E (MeV)	
	TRAJECTORY	CYCLONE	TRAJECTORY	CYCLONE	TRAJECTORY	CYCLONE
-45^0	.000000	.000000	.000000	.000000	.000040	.000040
-30^0	-.001385	-.001385	.016169	.016167	.011796	.011793
-15^0	-.011120	-.011119	.064683	.064675	.058065	.058050
0^0	-.039153	-.039147	.154503	.154486	.167267	.167229
15^0	-.096460	-.096442	.283363	.283334	.306805	.306750
30^0	-.190414	-.190384	.426737	.426698	.377333	.377287
45^0	-.323129	-.323084	.546580	.546543	.382733	.382690
60^0	-.482817	-.482757	.627917	.627888	.383095	.383052

small initial energy of 40 eV and the initial R.F. time was $\tau_0 = -45^o$. Some of the results are shown in Table 3.2. We see that, for the most part, we have agreement of position and energy to four significant figures. This is reasonably good considering the programs were written completely independently. One source of error is due to the fact that the version of CYCLONE used here automatically biases the ion source by (initial energy)/q, whereas in TRAJECTORY the ion source remains grounded. In the case ran here, this amounts to about a one part out of 10^4 difference in the voltage difference between source and puller.

Despite the small deviations here, (on the order of .01%) this comparison essentially verifies that TRAJECTORY is correctly and accurately solving the equations of motion.

3.4 Source to Puller Calculation in a Measured Electric Field

In this section TRAJECTORY will be used to study the energy gain and transit time across the first acceleration gap for various ions. These calculations will be similar to those of Reiser[11] in the respect that the results will be reported in terms of the dimensionless parameter χ defined by

$$\chi = \frac{\ell^2 B^2 q/m}{V} \tag{3.20}$$

where according to Reiser ℓ is a reference length, B the magnetic field strength at a reference point, q/m the charge to mass ratio for the ion, and V is a reference value of the voltages applied to the electrodes. The nice feature about reporting results in terms of χ is that for all systems having the same χ value, the ion trajectories through the system will be identical. (For relativistic motion, there is the additional

requirement that qV/m_0c^2 must be the same for the systems being compared.)

The difference between Reiser's calculations and the present ones is that Reiser assumes that both the magnetic and electric fields are homogeneous and here only the magnetic field will be assumed homogeneous. The electric field will be obtained from a previously measured grid of potentials for the source to puller region called 1.06.5-A.

A contour map of the potential arising from the geometry used is shown in Figure 3-3. The equipotential lines are 2% contours and extend from 2% to 98%. Superimposed on the figure are the trajectories for some of the cases studied here, and will be described later in the text.

In equation (3.20), ℓ will be taken as the source to puller gap width. If we define this as the distance from the ion source slit to a distance half way through the puller, then for field 1.06.5-A we have ℓ = .367 inch. For these studies we will also take the magnetic field strength to be 48.0 kG, which is a typical full field value in the central region of the K = 500 MeV cyclotron. The reference voltage will be taken as the maximum R.F. voltage on the puller electrode, which, in these studies, was taken as 100 kV. These values inserted into equation (3.20) give (adjusting the units properly)

$$\chi = 1.9317 \frac{q/e}{A} \tag{3.21}$$

Using TRAJECTORY, the energy at the puller electrode was obtained for several different χ values as a function of the R.F. starting time. For each χ-value, acceleration modes of h = 1, 2, 3, and 4 were studied. In TRAJECTORY, B and V were kept constant, q/e was taken to be 1.0 and the mass of the particle was adjusted using equation (3.21) to give the desired χ-value. All ions were given a small initial kinetic energy

of 40 eV.

The results of these calculations are shown in Figures 3-1 and 3-2 for χ-values of .05, .10, .15, .20, .30, .40, .50, and .60. The calculations were carried out at R.F. starting times ranging from $\tau_0 = -90^o$ (i.e., 90^o before peak voltage) to $\tau_0 = 0^o$ (peak voltage) in 5 R.F. degree step. Rather than plotting the energy at the puller for each ion, a quantity called ε is instead used, where ε is defined as

$$\varepsilon = \frac{E_{kin}}{q\Delta V}$$

Here ΔV is the voltage difference between the ion source slit and the location where the ion crosses the line ℓ = .367 inch (see Figure 3-3). Hence, ε represents the fraction of the total energy available in the source to puller region that the ion actually obtained. Note that because of the penetration of the voltages past the puller in the measured field, we will have $\Delta V \leq (100\ kV - V_{source})$, where the equality sign holds only in the cases where the ion trajectory actually touches or passes through the puller electrode.

Figures 3-1 and 3-2 exhibit features similar to those obtained by Reiser with the homogeneous electric field. That is, we observe a shift in the maximum energy gain to earlier starting times whenever h or χ is increased. Also, note the decrease in the number of ions that actually reach the puller for the higher harmonics as χ is increased (only those ions reaching the puller are plotted in the figures). For instance, when χ = .4, we see that no ions running in the mode h = 4 made it to the puller electrode. What happened to these ions was that the R.F. voltage was changing so rapidly that the electric field changed directions and pushed the particles back toward the source. Figure 3-3

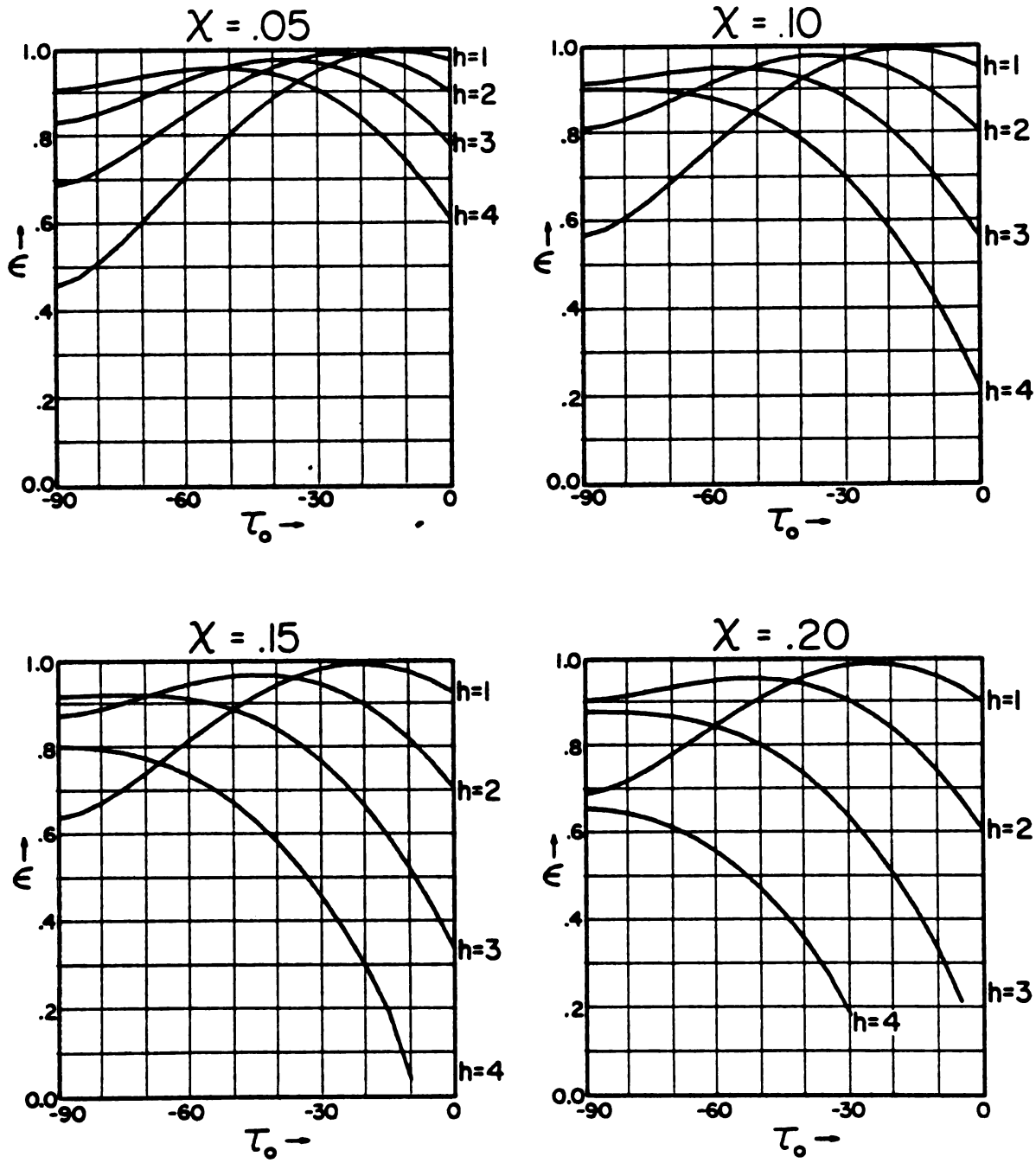

Figure 3-1.--$\varepsilon \equiv E_{kin}/q\Delta V$ at the puller vs. initial R.F. time for χ-values of .05, .10, .15, and .20. For each χ, curves are plotted for h = 1, 2, 3, and 4.

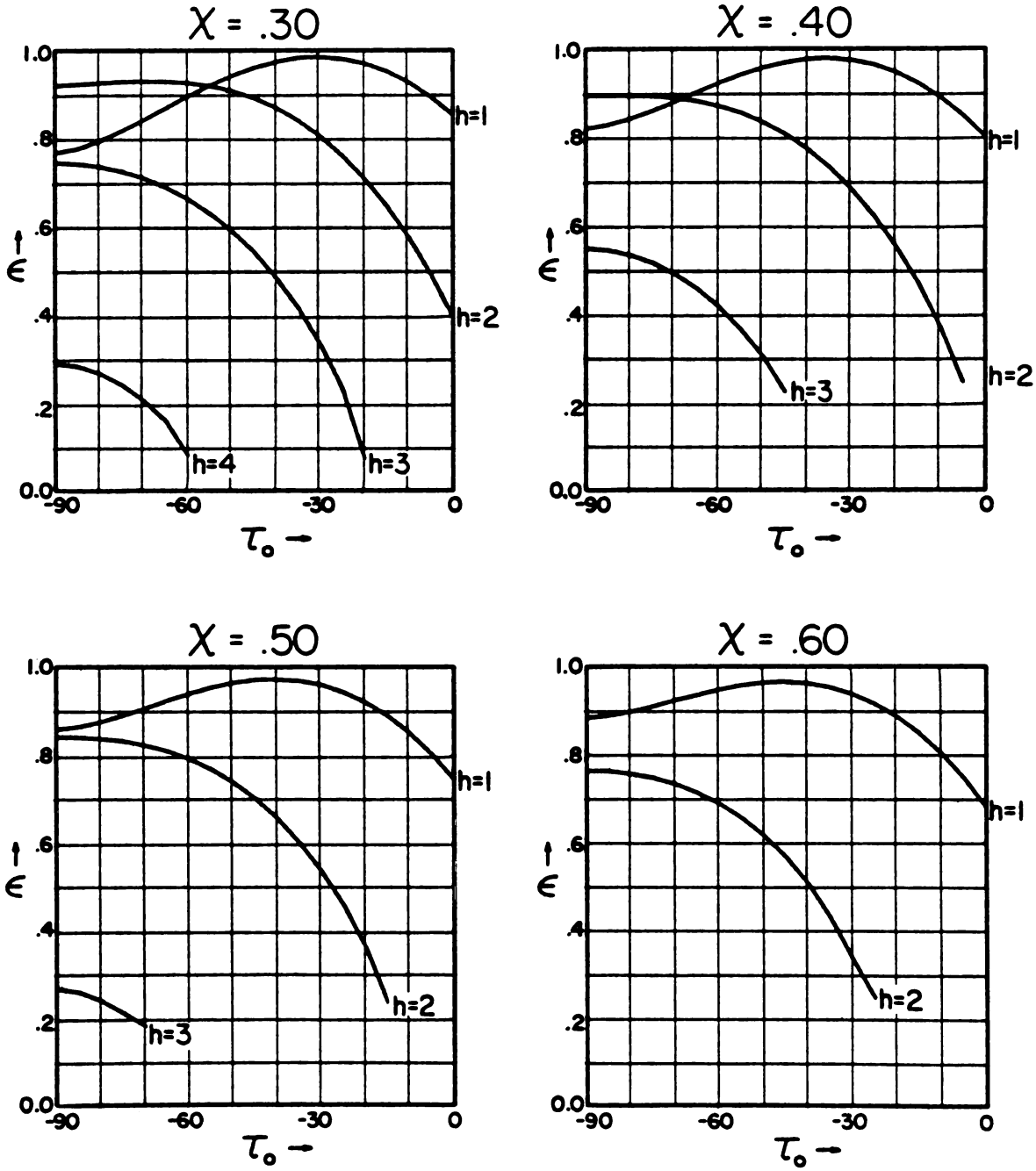

Figure 3-2.--$\varepsilon \equiv E_{kin}/q\Delta V$ at the puller vs. initial R.F. time for χ-values of .30, .40, .50, and .60. For each χ, curves are plotted for h = 1, 2, 3, and 4.

Figure 3-3.--Some predicted trajectories for ions with χ = .4 through field 1.06.5-A. The ions making it through the puller are running in the h = 1 mode, and those being pushed back to the source are running in the h = 4 mode. Both cases are plotted for R.F. starting times of $\tau_0 = -20^o$, -30^o, -40^o, and -50^o. The trajectories are superimposed on a 2% contour map of the equipotential lines. The scale is 8:1.

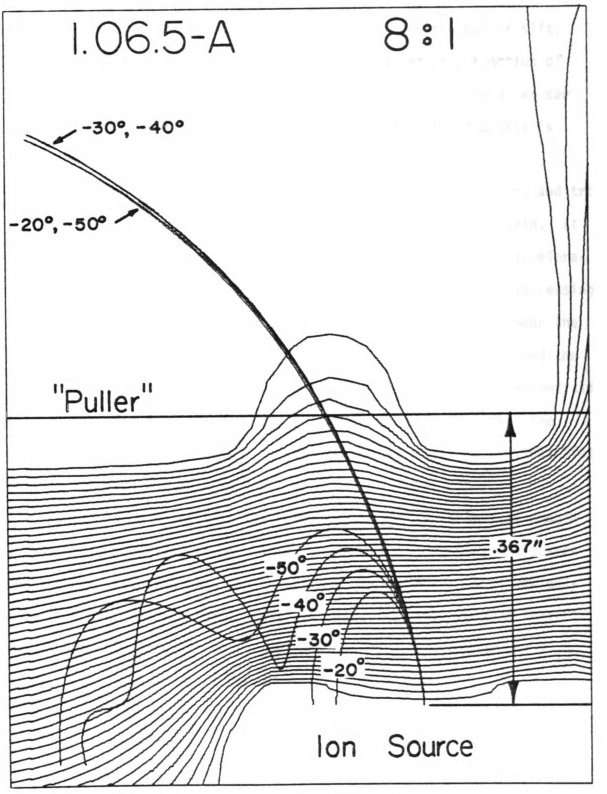

Figure 3-3

shows some of these difficult ion trajectories plotted on a contour map of the source to puller region being used. Also plotted are the trajectories for a case where the ions do make it through the puller slit.

Figure 3-4 plots $E_{kin}(max.) / q\Delta V$ at the puller as a function of χ for the modes of acceleration under study. From the figure, we see that the energy gain decreases with χ and the drop off in energy is especially pronounced in the higher acceleration modes.

Finally, Figure 3-5 plots the initial R.F. starting time τ_0 and transit time $\Delta\tau$ vs. χ for the cases that give the maximum energy gain. It can be seen that for increasing χ, the starting times in each acceleration mode are approaching $\tau_0 = -90^0$ with the rate of approach increasing with harmonic number. We also see that for each acceleration mode the transit time, $\Delta\tau = \tau_{puller} - \tau_{source}$, goes up with increasing χ and the rate of increase goes up with harmonic number. These results essentially tell us that for increasing χ and/or increasing harmonic number the particles want to spend more R.F. time in the accelerating electric field in order to gain the most energy.

It should be noted that the curves of Figure 3-5 aren't as smooth as one would hope them to be. This is due to the fact that the search for the R.F. starting time that gives the maximum energy gain was only made in 5 R.F. degree steps. That is, the points used to plot these curves are only accurate to ±5 R.F. degrees in τ_0. And since $\Delta\tau = \tau_{puller} - \tau_0$, the $\Delta\tau$ vs. χ curves are also affected.

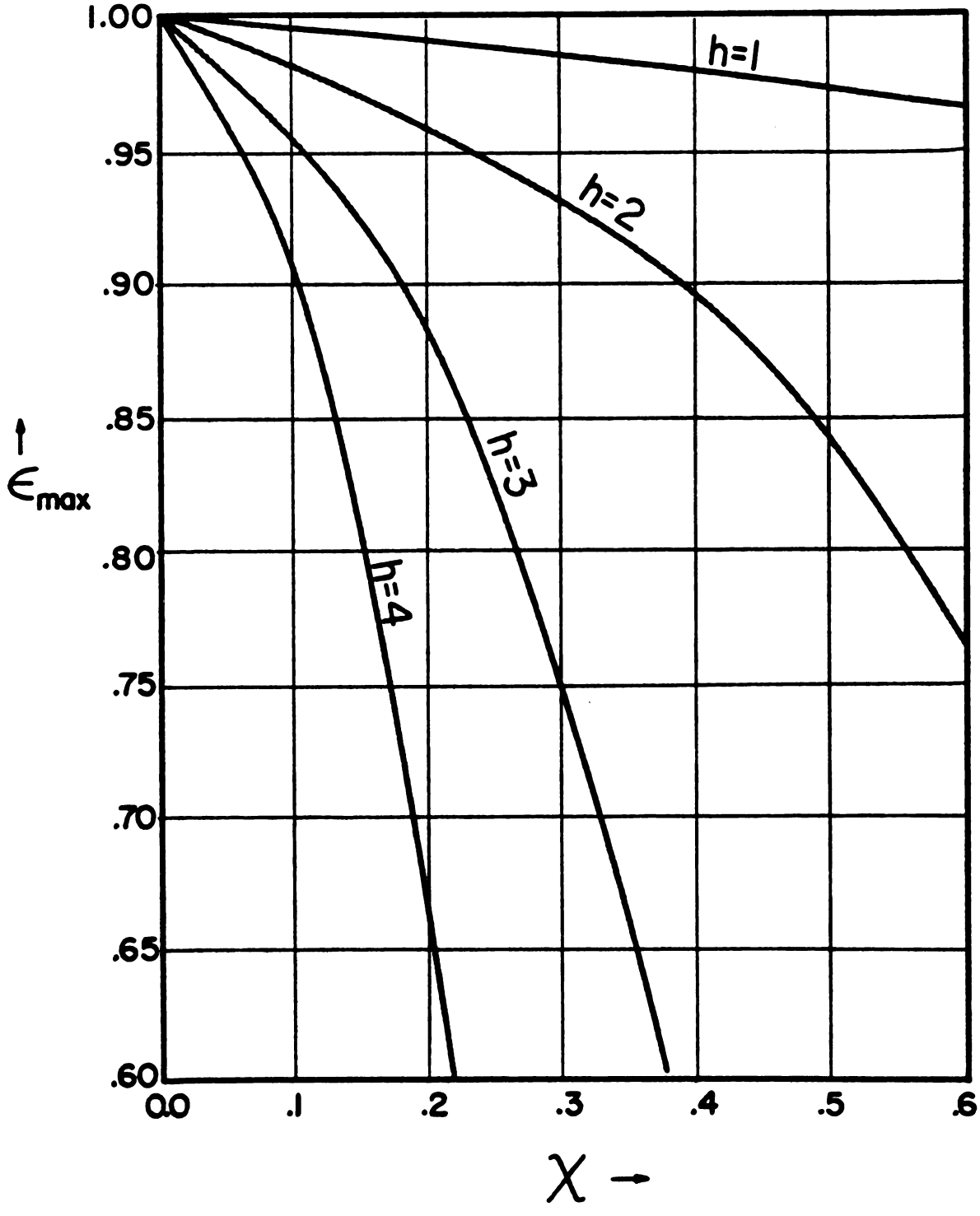

Figure 3-4.--Maximum ε at the puller vs. χ for accelerating modes of h = 1, 2, 3, and 4.

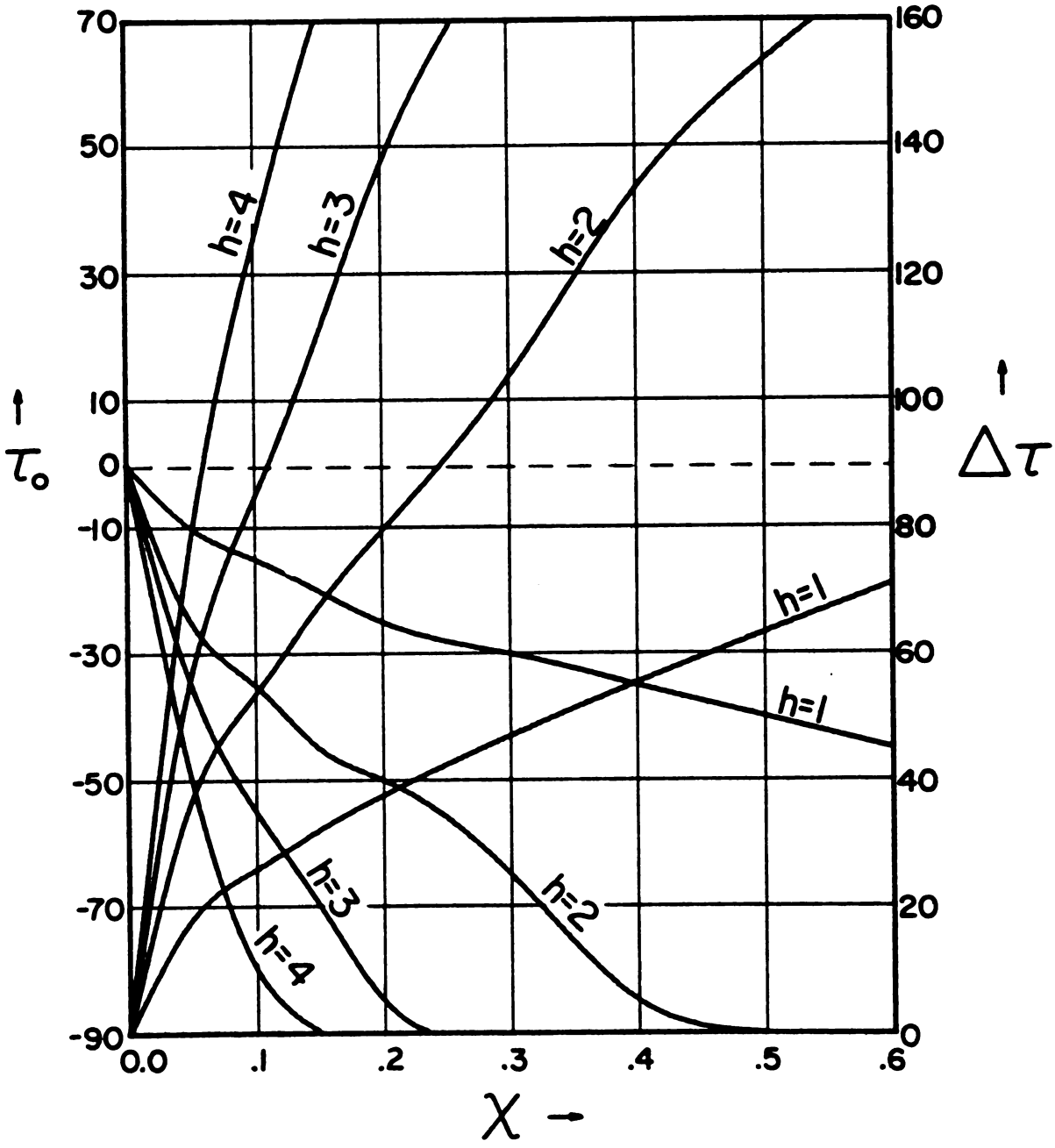

Figure 3-5.--Initial R.F. time τ_0 and transit time $\Delta\tau$ vs. χ for the cases that give maximum source to puller energy gain. Results are again shown for h = 1, 2, 3, and 4.

LIST OF REFERENCES

LIST OF REFERENCES

1. B. T. Smith, "Magnetic Field Due to a Circular Current," M.S. thesis, Michigan State University, 1960.

2. M. Gordon, Private Communication.

3. I. S. Gradshteyn and I. M. Ryzhik, Table of Integrals, Series, and Products, Academic Press, 1965, p. 907.

4. IBM Scientific Subroutines, Modified by L. Fellingham for use on the Michigan State University Cyclotron Laboratory's Xerox Sigma-Seven computer, 1971.

5. M. Abramowitz and I. A. Stegun (eds.), Handbook of Mathematical Functions, Dover Publications, 1972, p. 597 ff.

6. L. V. King, On the Direct Numerical Calculations of Elliptic Functions and Integrals, Cambridge at the University Press, 1924.

7. D. Johnson, WIRE FIELD, Michigan State University Cyclotron Laboratory.

8. M. Gordon and D. Johnson, SPIRAL GAP, Michigan State University Cyclotron Laboratory.

9. A. Ralston and H. Wilf (eds.), Mathematical Methods for Digital Computers, Wiley and Sons, Inc., 1967, M. Romanelli, "Runga Kutta Methods for the Solution of Ordinary Differential Equations," pp. 110-120.

10. M. Abramowitz and I. A. Stegun (eds.), p. 879.

11. M. Reiser, "Central Orbit Program for a Variable Energy Multi-Particle Cyclotron," Nuclear Instruments and Methods, 18, 19, 1962, pp. 370-377.